Size-Controlled Cobalt Nanoplates and Their Impact on Oxygen Evolution Catalysis

Zeno Rizqi Ramadhan,[a,c] Agus R. Poerwoprajitno,[b] Soshan Cheong,[c] J. Justin Gooding,*[a,d] Richard Tilley*[a,c,d]

[a] Dr. Z. R. Ramadhan, Prof. Dr. J. J. Gooding, Prof. Dr. R. D. Tilley
School of Chemistry
The University of New South Wales
Sydney, NSW 2052 (Australia)
E-mail: r.tilley@unsw.edu.au; justin.gooding@unsw.edu.au

[b] Dr. A. R. Poerwoprajitno
Center for Integrated Nanotechnologies
Sandia National Laboratories
Albuquerque, NM 87185, USA.

[c] Dr. Z. R. Ramadhan, Dr. S. Cheong, Prof. Dr. R. D. Tilley
Mark Wainwright Analytical Centre
The University of New South Wales
Sydney, NSW 2052 (Australia)

[d] Prof. Dr. J. J. Gooding, Prof. Dr. R. D. Tilley
Australian Centre for NanoMedicine
The University of New South Wales
Sydney, NSW 2052 (Australia)

Supporting information and ORCID identification number(s) for author(s) for this article can be found under:
http://doi.org/xxxx

Abstract: Controlling the size of nanoparticles is important in catalytic reactions, not only for tuning the surface area but also for modifying the electronic structure. However, achieving precise size control in two-dimensional (2D) structures remains challenging. In this work, we demonstrate precise size control of cobalt nanoplates, ranging from 19 nm to 80 nm, which is achieved by tuning the ratio of two surfactants used in the synthesis. The 19 nm of Co nanoplates exhibit higher oxygen evolution reaction activity due to a higher proportion of $\{10\bar{1}1\}$ to {0001} facet. This size control allows systematic investigation into how nanoplate dimensions influence catalytic performance in the oxygen evolution reaction, offering new insights into structure activity relationships of cobalt nanocatalysts.

1. Introduction

Tuning the nanoparticle size is an effective strategy not only for increasing electrochemically active surface area (ECSA) but also maximizing the exposure of specific active sites in the case of anisotropic nanoparticles, such as branches, plates and rods.[1] While precise size control has been well-established for spherical nanoparticles,[2] achieving similar control over anisotropic nanoparticles remains challenging.

Cobalt-based materials are among the most promising non-noble catalysts for for many catalytic reactions, for example the oxygen evolution reaction (OER) which is a bottleneck reaction in the water splitting process.[3] Cobalt oxyhydroxide species ($CoO_x(OH)_y$) act as the active site of cobalt during the OER process.[4] Co is widely reported as an active OER catalyst and smaller Co nanoparticles have been shown to enhance OER catalytic activity by increasing Co-O contraction, indicating that well-controlled particle size is critical for catalytic activity.[5]

One particularly interesting anisotropic shape is the two-dimensional (2D) nanoplate, which offers a high surface area-to-volume ratio, an important feature for catalytic applications.[6] Although Co nanoplates have been successfully synthesized in previous studies, precise control over their dimensions remains a significant synthetic challenge.

Here, we present a facile one-pot synthesis method for controlling the size of Co nanoplates, ranging from 19 nm to 80 nm. The size control is achieved by varying the ratio of two surfactants used during synthesis. This high degree of tunability allows for a systematic investigation of the relationship between nanoplate size and OER activity.

2. Experimental Section

2.1. Synthesis of Co nanoplates

80 mg Chlorotris(triphenylphosphine)cobalt(I) ($CoCl(PPh_3)_3$) (Sigma Aldrich, 97%), hexadecylamine (HDA) (Sigma Aldrich, 98%) and lauric acid (LA) (Sigma Aldrich, 98%) were dissolved in 3 mL anisole anhydrous (Sigma Aldrich, 99.7%) in a vial. The ratio between HDA and LA surfactant can be tuned to control the diameter of nanoplates. The 19 nm used HDA (0.23 mmol) and LA (0.11 mmol), 42 nm used HDA (0.15 mmol) and LA (0.11 mmol), and 80 nm used HDA (0.15 mmol) and LA (0.19 mmol). The solution was prepared in the glove box and then transferred into a Fisher-Porter bottle. The bottle was filled with 3 bars of hydrogen gas and placed in an oil bath at 150°C. After 48 hours, the bottle was cooled down, and the hydrogen was released. After the reaction, the product was washed using toluene and separated by magnetic force and redissolved in toluene in the glove box to make sure the excess surfactant was removed. For catalytic measurements, the nanoparticles were loaded on Vulcan XC-72 carbon (Fuel Cell Store).

2.2. Characterization

Transmission Electron Microscope (TEM) and Fast Fourier Transforms (FFTs) images were taken on JOEL JEM F200 Multi-Purpose FEG TEM operating at 200 kV. The crystal structure of Co nanoplates was analyzed by X-ray Diffraction (XRD) (Empyrean 2 PANanalytical) using a Co Kα X-ray tube to minimize fluorescence.

2.3 Electrochemical measurements

The electrochemical oxygen evolution reaction was evaluated in a three-electrode cell using 1 M KOH as the electrolyte with Pt plate as counter electrode and Hg|HgO in 1 M NaOH as a reference electrode. The working electrode was prepared by drop-cast of a catalyst ink which was prepared by dispersing the Co nanoplates/C sample with water, isopropyl alcohol (IPA), and Nafion® with a ratio of 70:28:2 vol%. The concentration of ink was 2.5 mg mL^{-1}. The final catalyst loading was 0.1 mg/ml as determined by Inductively Coupled Plasma Optical Emission Spectroscopy (ICP-OES, Perkin Elmer Optima). The measurements were performed using a Solartron SI 1287 electrochemical interface and SI 1260 impedance/grain-phase analyzer. The working electrode kept rotating at 1600 rpm during the experiments. Pre-treatment was performed by potential cycling between 0.8 V and 1.55 V vs RHE for 30 cycles for catalyst activation.

All potentials were given relative to the reversible hydrogen electrode (RHE) according to the equation:

$$E_{RHE} = E_{Hg|HgO|1\ M\ NaOH} + 0.059 \times pH + E^0_{Hg|HgO|1\ M\ NaOH}$$

The electrochemical impedance spectroscopy (EIS) was performed with a Solartron SI 1287 electrochemical interface and SI 1260 impedance/grain-phase analyzer in a frequency range of 10^6 to 10^{-1} Hz and AC amplitude of 10 mV. The fitting for EIS spectra was done using two-time constant (R(QR)(QR)) as shown in Figure S6 using the "ZSmip.Win 3.22" software. The charge transfer resistance of the OER process was measured at a semi-circle at a lower frequency. Stability test was performed by chronopotentiometry at 10 mA cm^{-2}. The particles were loaded in carbon cloth, and the electrolyte was stirred to remove the bubbles in the carbon cloth.

The turnover frequency (TOF) value for OER was described following this equation:

$$TOF = j/(n \times C)$$

$$Number\ of\ active\ sites = C/F$$

Where i is the current at 1.57 V vs RHE, n is the number of electrons transferred (for OER is 4), C is the charge of Co^{4+} to Co^{3+} reduction, and F is the Faraday constant (96500 C mol^{-1}). The charge (C) of Co^{4+} to Co^{3+} reduction was calculated by integrating the area of current (A) over time (s) in the Co^{4+} to Co^{3+} reduction potential.[7]

3. Results and Discussion

To synthesize Co nanoplate, $CoCl(PPh_3)_3$, hexadecylamine, lauric acid, and anhydrous anisole were mixed and reacted at 150 °C under 3 bar H_2 in a Fisher-Porter bottle. The reaction was left for 48 h to ensure that the precursor was reacted completely. The uniform shape of Co nanoplates is revealed in the TEM images in Figure 1a. The different shapes of hexagons and elongated hexagons are due to different orientations of particle.[8]

The size of Co nanoplates was controlled by adjusting the ratio of LA to HDA surfactants from 0.5 to 1.2. A linear relationship was obtained between the surfactant ratio and nanoplate diameter (Figure 1b). As the LA:HDA ratio increased, the diameter of the Co nanoplates increased from 19 ± 5 nm (0.5 ratio) to 42 ± 7 nm (0.7 ratio) and 80 ± 15 nm (1.2 ratio). In contrast, the thickness remained relatively constant in the range of 13 – 19 nm (Figure S1).

Changing the surfactant ratio alters the growth mechanism of the Co nanoplates. Increasing the LA:HDA ratio improves the proportion of carboxylic acid groups that preferentially bind to the top and bottom surfaces of the

nanoplates. This selective binding promotes lateral growth by directing additional atom deposition onto the side faces, resulting in larger nanoplates with relatively constant thickness.[9] The HDA or LA is only present in the synthesis that results in the non-plate shape, indicating that the HDA and LA are important for forming plate-shaped particles (Figure S2 and S3). N-hexadecyl laurylamide, as a condensation of HDA and LA, is expected to act as a surfactant involved in the formation of the plate-shaped particle.[10]

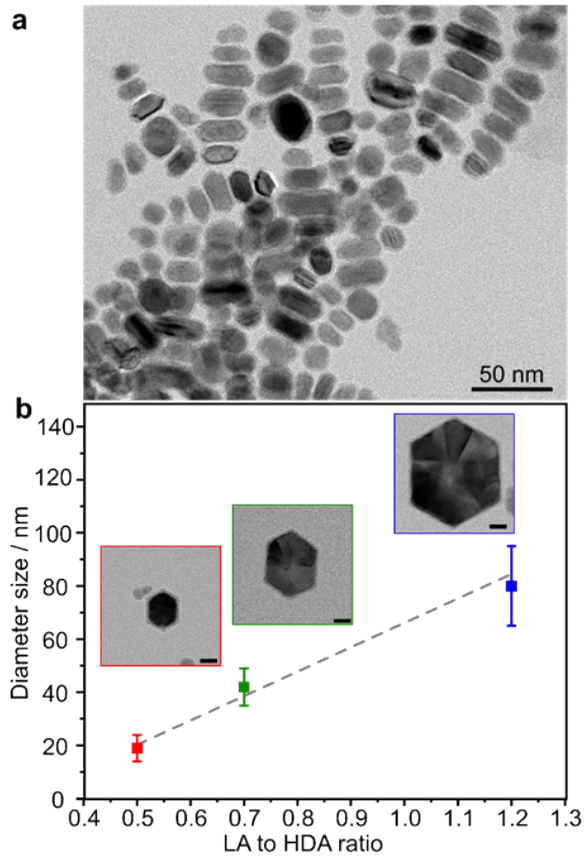

Figure 1. (a) TEM image of Co nanoplates with a length size distribution of 19 nm, (b) The LA to HDA ratio versus the diameter of Co nanoplates, with a representative TEM image of each sample. The scale bars are 20 nm.

The Co nanoplates adopt a pure hexagonal close-packed (hcp) crystal structure, as confirmed by X-ray diffraction (Figure S4, SI) and selected area electron diffraction (SAED) patterns. The SAED rings can be indexed to the $(10\bar{1}0)$, (0002), and $(10\bar{1}1)$ planes (Figure S4, SI). The key to forming single-crystalline hcp Co nanoparticles lies in the use of H_2 as a mild reducing agent. This ensures the slow reduction of the cobalt precursor, allowing Co atoms to gradually arrange into a well-ordered, single-crystal structure.[11]

The electrocatalytic behaviour of Co nanoplates was evaluated in a 1 M KOH electrolyte. Cyclic voltammetry (CV) was performed using a rotating glassy carbon electrode, sweeping from 0.95 V to 1.64 V vs. RHE for 30 cycles to activate the nanoparticle surface. Two pairs of redox peaks were observed at approximately 1.1 V and 1.4 V, corresponding to the Co^{2+}/Co^{3+} and Co^{3+}/Co^{4+} redox transitions, respectively (Figure S5). A smooth increase in current was observed at potentials above 1.52 V vs. RHE, which is attributed to the onset of the OER. This activation process results in the surface reconstruction that creates oxyhydroxide species around 3-6 nm in thickness on the surface of nanoparticles as a passivation layer.[12] This activation process was conducted on all

different sizes of Co nanoplates, which are expected to have a similar oxyhydroxide structure on their surface. These results indicate that Co nanoplates are promising candidates for OER catalysis.[12a, 13]

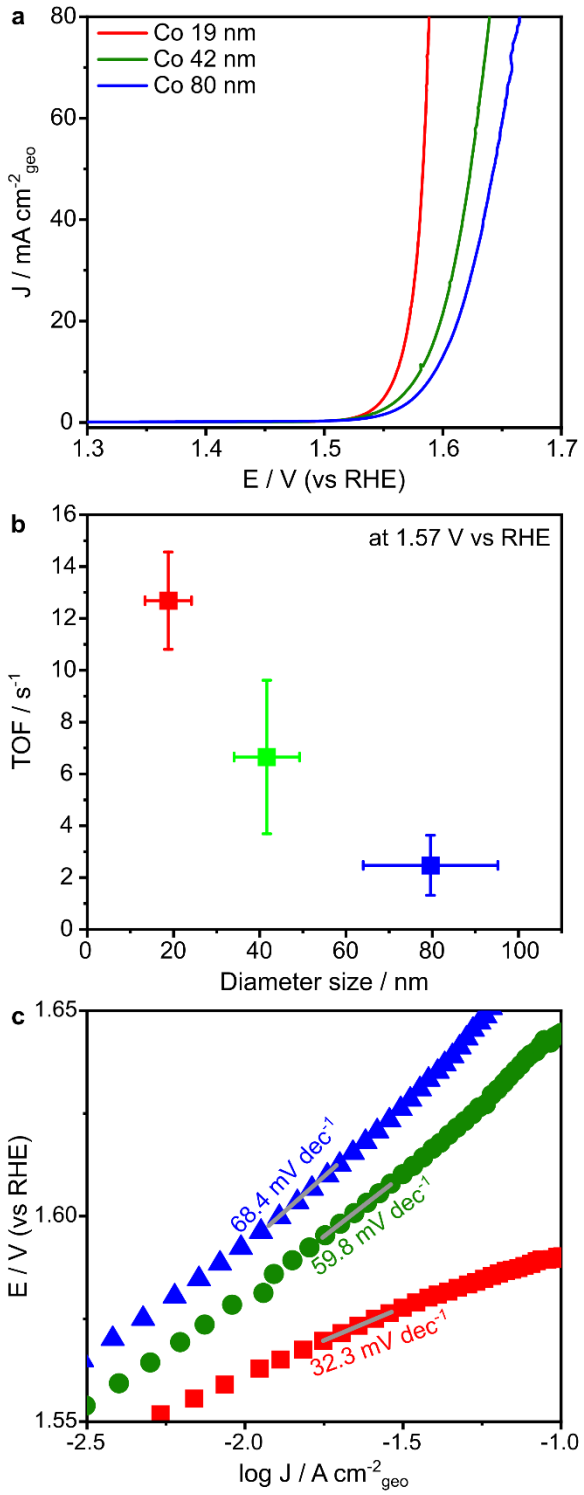

Figure 2. (a) LSV of Co nanoplates with different diameter sizes in 1 M KOH with a scan rate of 10 mV s^{-1}. (b) TOF value at 1.57 V vs RHE versus various diameter sizes of Co nanoplatelets. (c) Tafel plots analysis for various diameter sizes of Co nanoplates.

The OER performance of the Co nanoplates was evaluated using linear sweep voltammetry (LSV) as shown in Figure 2a, which demonstrates that the 19 nm nanoplates deliver the lowest overpotential of 330 mV at 10 mA cm^{-2}, compared to the 42 nm (350 mV) and 80 nm (363 mV) nanoplates. While the Co nanoplates have lower overpotential compared to Co-based nanoparticles indicating the Co nanoplates are good catalysts for OER (Table S2). From the LSV in Figure 2a, the 19 nm Co nanoplates reach ~80 mA cm^{-2}, suggesting promise for industrially relevant current densities. The intrinsic activity of the Co nanoplates was evaluated by the TOF, where the number of moles of cobalt active sites on the surface that are involved in the reaction was derived from the integration of

the Co^{4+} to Co^{3+} reduction peak (Figure S6).[7a, 14] The 19 nm Co nanoplates catalyst exhibits a higher TOF value of 12.7 s^{-1}, which is 5.1 and 2.7 times more active than the 42 nm (6.7 s^{-1}) and 80 nm (2.5 s^{-1}) nanoplates (Figure 2b).

The 19 nm Co nanoplates exhibit different reaction mechanisms and enhanced reaction kinetics by showing reduced charge transfer resistance. The 19 nm Co nanoplates achieve a lower Tafel slope of 32.3 mV dec^{-1} compared to the 42 nm (59.7 mV dec^{-1}) and 80 nm (68.4 mV dec^{-1}) nanoplates, as shown in Figure 2c. The 42 nm and 80 nm Co nanoplates have similar Tafel slope values as those of bulk Co oxides of ~60 mV dec^{-1},[15] while the 19 nm has a much smaller Tafel slope value implying a different rate-determining step for M-O formation (~60 mV dec^{-1}) and O-O formation (~40 mV dec^{-1}), due to a different proportion of side to top faces resulting from a smaller diameter of the Co nanoplates.[14, 16] The reduction of charge transfer resistance is demonstrated by EIS measured at the OER regime. The Nyquist plot shows that the 19 nm nanoplates exhibit a smaller charge transfer resistance (R_{ct}) of 11.9 Ω for OER, compared to the 42 nm (22.9 Ω) and 80 nm (26.1 Ω) nanoplates (Figure S7 and Table S3). This smaller R_{ct} value of the 19 nm Co nanoplates is attributed to the large number of active sites in the nanoparticles, resulting in faster charge transfer.[17] This higher number of active sites is due to a higher proportion ratio of side to top faces in the nanoparticles compared to those of 42 and 80 nm. As the nanoplates have identical crystal structure and chemical composition (Figure S8), the improvement in OER activity is attributed to having smaller nanoplate sizes.

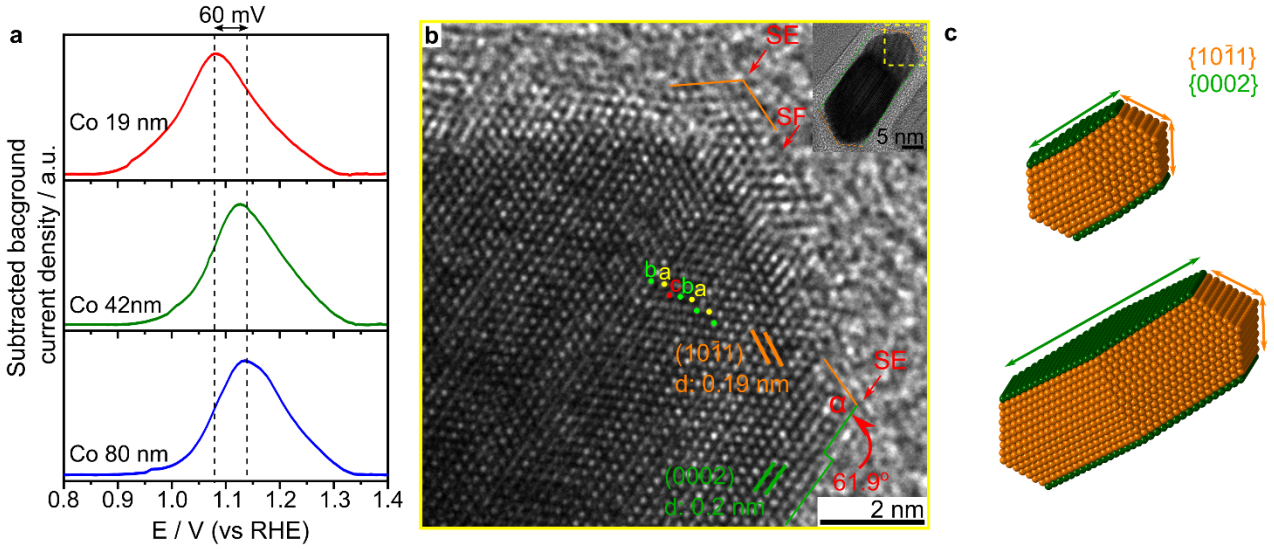

Figure 3. (a) Background-subtracted LSV of various diameter sizes of Co nanoplates at the Co^{2+} to Co^{3+} oxidation potential range. (b) High resolution TEM (HRTEM) image of Co nanoplate viewed down <010> direction. (c) Atomic models showing the surface faceting on Co nanoplates. Green and orange colour atoms represent Co atoms on {0001} facets and {10$\bar{1}$1} facets.

The high activity of the 19 nm Co nanoplates are attributed to their ability to form active Co sites at lower potentials. The background-subtracted current density from the Co oxidation peak shows that the 19 nm Co nanoplates oxidize Co^{2+} to Co^{3+} at a potential 60 mV more negative than the 80 nm Co nanoplates (Figure 3a). The generation of more active Co^{3+} sites at lower potentials drives the OER at lower overpotentials, due to their high electrochemically active surface area on the lateral side. The surface of nanoplates consists of {10$\bar{1}$1} and {0001} facets on the lateral and top side (Figure 3b and Figure S9-10), the higher proportion of {10$\bar{1}$1} facet compared to {0001} facet shows better catalytic activity because it is dominated by low-coordinated atoms, which facilitate the deprotonation process, thereby driving the formation of Co^{3+} (Figure 3c, Figure S11 and Table S4.).[12a, 18] This influence of surface facets has been successfully shown to improve catalytic reaction in several Co-based and Ni materials.[1b, 14-15]

The less energy required to form an active Co site is due to the high proportion of Co atoms on the {10$\bar{1}$1} facets and defects, such as step-edges and stacking faults (denoted SE and SF in Figure 3b) which a key active sites for OER.[7b, 15a] These defects are atomic step-edge made of n(10$\bar{1}$1) x n(10$\bar{1}$1) and n(10$\bar{1}$1) x n(0001) and stacking faults help in adsorption of OER intermediates and facilitate deprotonation due to in presence of low-coordinated atoms, which have been shown to improve efficiency for electrocatalytic reactions.[19]

The 19 nm Co nanoplates also exhibit excellent long-term stability, as demonstrated by chronopotentiometry measurement at a constant current density of 10 mA cm^{-2}, where the catalyst was maintained for 8 h at a potential of ~1.56 V vs RHE (Figure S12). The stability of the Co nanoplates can be attributed to the low-index facets, which have been shown to be stable under OER conditions.[20]

4. Conclusion

In conclusion, we demonstrate that the size of Co nanoplates can be precisely controlled by adjusting the ratio between the two surfactants. Increasing the LA to HDA ratio promotes lateral growth while maintaining constant thickness, resulting in a larger diameter. Among the samples, Co nanoplates with a diameter of 19 nm exhibit the highest OER activity, outperforming those with diameters of 42 nm and 80 nm. This enhanced performance is attributed to a greater exposure of the $\{10\bar{1}1\}$ facet and a higher density of defects, such as stacking faults, atomic steps, and edge atoms. This strategy provides a versatile platform for synthesizing well-defined nanoplates tailored for a variety of catalytic applications.

Acknowledgements

This work was supported by the Australian Research Council's Discovery Project grants awarded to R.D.T. (DP230100596, DP250100915, and CE230100032) and J.J.G. (DP210102698). The authors acknowledge facilities supported by Microscopy Australia at the Electron Microscope Unit at UNSW. This work was performed, in part, at the Center for Integrated Nanotechnologies, an Office of Science User Facility operated for the U.S. Department of Energy (DOE) Office of Science. Sandia National Laboratories is a multimission laboratory managed and operated by National Technology & Engineering Solutions of Sandia, LLC, a wholly owned subsidiary of Honeywell International, Inc., for the U.S. DOE's National Nuclear Security Administration under contract DE-NA-0003525. The views expressed in the article do not necessarily represent the views of the U.S. DOE or the United States Government.

Conflict of interest

The authors declare no conflict of interest.

Keywords: nanoplate particles • electrocatalysis • oxygen evolution reaction • surface facet • defect

[1] a) A. R. Poerwoprajitno, S. Cheong, L. Gloag, J. J. Gooding, R. D. Tilley, *Acc. Chem. Res.* **2022**, *55*, 1693-1702; b) A. R. Poerwoprajitno, L. Gloag, J. Watt, S. Cychy, S. Cheong, P. V. Kumar, T. M. Benedetti, C. Deng, K.-H. Wu, C. E. Marjo, D. L. Huber, M. Muhler, J. J. Gooding, W. Schuhmann, D.-W. Wang, R. D. Tilley, *Angew. Chem. Int. Ed.* **2020**, *59*, 15487-15491.

[2] a) Z. Li, D. He, X. Yan, S. Dai, S. Younan, Z. Ke, X. Pan, X. Xiao, H. Wu, J. Gu, *Angew. Chem. Int. Ed.* **2020**, *59*, 18572-18577; b) C. Stanglmair, S. P. Scheeler, C. Pacholski, *Eur. J. Inorg. Chem* **2014**, *2014*, 3633-3637.

[3] a) C. Huang, P. Qin, Y. Luo, Q. Ruan, L. Liu, Y. Wu, Q. Li, Y. Xu, R. Liu, P. K. Chu, *Mater. Today Energy* **2022**, *23*, 100911; b) M. Yu, E. Budiyanto, H. Tüysüz, *Angew. Chem. Int. Ed.* **2022**, *61*, e202103824; cY. Lu, T. Liu, C.-L. Dong, C. Yang, L. Zhou, Y.-C. Huang, Y. Li, B. Zhou, Y. Zou, S. Wang, *Adv. Mater.* **2022**, *34*, 2107185.

[4] a) F. Reikowski, F. Maroun, I. Pacheco, T. Wiegmann, P. Allongue, J. Stettner, O. M. Magnussen, *ACS Catal.* **2019**, *9*, 3811-3821; b) A. Bergmann, T. E. Jones, E. Martinez Moreno, D. Teschner, P. Chernev, M. Gliech, T. Reier, H. Dau, P. Strasser, *Nat. Catal.* **2018**, *1*, 711-719.

[5] F. T. Haase, A. Bergmann, T. E. Jones, J. Timoshenko, A. Herzog, H. S. Jeon, C. Rettenmaier, B. R. Cuenya, *Nat. Energy* **2022**, *7*, 765-773.

[6] L. Gloag, A. R. Poerwoprajitno, S. Cheong, Z. R. Ramadhan, T. Adschiri, J. J. Gooding, R. D. Tilley, *Sci. Adv.* **2023**, *9*, eadf6075.

[7] a) L. Yu, S. Sun, H. Li, Z. J. Xu, *Fundam. Res.* **2021**, *1*, 448-452; b) Z. R. Ramadhan, A. R. Poerwoprajitno, S. Cheong, R. F. Webster, P. V. Kumar, S. Cychy, L. Gloag, T. M. Benedetti, C. E. Marjo, M. Muhler, D.-W. Wang, J. J. Gooding, W. Schuhmann, R. D. Tilley, *J. Am. Chem. Soc.* **2022**, *144*, 11094-11098.

[8] J. S. Evans, C. N. Beier, I. I. Smalyukh, *J. Appl. Phys.* **2011**, *110*.

[9] A. R. Poerwoprajitno, L. Gloag, S. Cheong, J. J. Gooding, R. D. Tilley, *Nanoscale* **2019**, *11*, 18995-19011.

[10] K. Kaźmierczak, D. Yi, A. Jaud, P.-F. Fazzini, M. Estrader, G. Viau, P. Decorse, J.-Y. Piquemal, C. Michel, M. Besson, K. Soulantica, N. Perret, *J. Phys. Chem. C* **2021**, *125*, 7711-7720.

[11] a) A. Moisset, A. Sodreau, A. Vivien, C. Salzemann, P. Andreazza, S. Giorgio, M. Petit, C. Petit, *Nanoscale* **2021**, *13*, 11289-11297; bF. Dumestre, B. Chaudret, C. Amiens, M.-C. Fromen, M.-J. Casanove, P. Renaud, P. Zurcher, *Angew. Chem. Int. Ed.* **2002**, *41*, 4286-4289.

[12] a) C. Luan, J. Angona, A. Bala Krishnan, M. Corva, P. Hosseini, M. Heidelmann, U. Hagemann, E. Batsa Tetteh, W. Schuhmann, K. Tschulik, T. Li, *Angew. Chem. Int. Ed.* **2023**, *62*, e202305982; b) T. Wu, S. Sun, J. Song, S. Xi, Y. Du, B. Chen, W. A. Sasangka, H. Liao, C. L. Gan, G. G. Scherer, L. Zeng, H. Wang, H. Li, A. Grimaud, Z. J. Xu, *Nat. Catal.* **2019**, *2*, 763-772; c) J. Xu, C.-C. Kao, H. Shen, H. Liu, Y. Zheng, S.-Z. Qiao, *Angew. Chem. Int. Ed.* **2025**, *64*, e202420615.

[13] A. Bergmann, E. Martinez-Moreno, D. Teschner, P. Chernev, M. Gliech, J. F. de Araújo, T. Reier, H. Dau, P. Strasser, *Nat. Commun.* **2015**, *6*, 8625.

[14] Z. Liu, H. M. A. Amin, Y. Peng, M. Corva, R. Pentcheva, K. Tschulik, *Adv. Funct. Mater.* **2022**, *33*, 2210945.

[15] a) S. Wang, Q. Jiang, S. Ju, C.-S. Hsu, H. M. Chen, D. Zhang, F. Song, *Nat. Commun.* **2022**, *13*, 6650; b) A. Moysiadou, S. Lee, C.-S. Hsu, H. M. Chen, X. Hu, *J. Am. Chem. Soc.* **2020**, *142*, 11901-11914.

[16] a) J. T. Mefford, A. R. Akbashev, M. Kang, C. L. Bentley, W. E. Gent, H. D. Deng, D. H. Alsem, Y.-S. Yu, N. J. Salmon, D. A. Shapiro, P. R. Unwin, W. C. Chueh, *Nature* **2021**, *593*, 67-73; b) S. Saddeler, U. Hagemann, S. Schulz, *Inorg. Chem.* **2020**, *59*, 10013-10024.

[17] H.-F. Zhao, J.-Q. Yao, Y.-S. Wang, N. Gao, T. Zhang, L. li, Y. Liu, Z.-J. Chen, J. Peng, X.-W. Liu, H.-B. Yu, *Adv. Sci.* **2024**, *11*, 2404095.

[18] J. Chen, A. Selloni, *J. Phys. Chem. C* **2013**, *117*, 20002-20006.

[19] a) F. Ikram, S. Cheong, I. Persson, Z. R. Ramadhan, A. R. Poerwoprajitno, J. J. Gooding, R. D. Tilley, *J. Am. Chem. Soc.* **2025**, *147*, 10784-10790; b) Q. Zhu, Z. Pan, Z. Zhao, G. Cao, L. Luo, C. Ni, H. Wei, Z. Zhang, F. Sansoz, J. Wang, *Nat. Commun.* **2021**, *12*, 558.

[20] A. R. Poerwoprajitno, L. Gloag, T. M. Benedetti, S. Cheong, J. Watt, D. L. Huber, J. J. Gooding, R. D. Tilley, *Small* **2019**, *15*, e1804577.

Entry for the Table of Contents

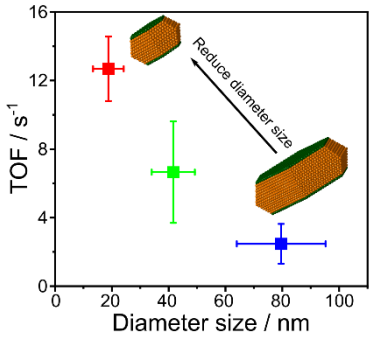

Cobalt nanoplate nanoparticles with controlled diameter size are presented to enhance catalytic activity for the oxygen evolution reaction. This improvement is attributed to a high proportion of $\{10\bar{1}1\}$ surface facets and the presence of defects such as step-edges and stacking faults.